A Low-Power Stand-Alone Adaptive Circuit for Harvesting Energy From a Piezoelectric Micropower Generator

Ahmadreza Tabesh, *Member, IEEE*, and Luc G. Fréchette, *Member, IEEE*

***Abstract*—An adaptive energy-harvesting circuit with low power dissipation is presented and demonstrated, which is useful for efficient ac/dc voltage conversion of a piezoelectric micropower generator. The circuit operates stand-alone, and it extracts the piezoelectric strain energy independent of the load and piezoelectric parameters without using any external sensor. The circuit consists of a voltage-doubler rectifier, a step-down switching converter, and an analog controller operating with a single supply voltage in the range of 2.5–15 V. The controller uses the piezoelectric voltage as a feedback and regulates the rectified voltage to adaptively improve the extracted power. The nonscalable power dissipation of the controller unit is less than 0.05 mW, and the efficiency of the circuit is about 60% for output power levels above 0.5 mW. Experimental verifications of the circuit show the following: 1) the circuit notably increases the extracted power from a piezoelectric element compared to a simple full-bridge diode rectifier without control circuitry, and 2) the efficiency of the circuit is dominantly determined by its switching converter. The simplicity of the circuit facilitates the development of efficient piezoelectric energy harvesters for low-power applications such as wireless sensors and portable devices.**

***Index Terms*—Energy harvesting, energy scavenging, low-power energy conversion, piezoelectric generator, power management circuit, stand-alone energy harvester.**

I. Introduction

PIEZOELECTRIC energy harvesters are vibrating devices that convert mechanical strain energy into electricity. Centimeter-scale piezoelectric elements can generate milliwatt-range electric power using ambient vibrations below 1 kHz. They have recently been considered as viable solutions for long-life micropower generators since they generate sufficient power to drive low-power electronic devices such as smart wireless sensors that consume less than a few milliwatts [1]–[5]. A vibrating piezoelectric element electrically behaves as a capacitive ac source [6], [7] which must be rectified at a desired dc voltage level to be useful for powering an electronic device. A diode rectifier connected to a battery is the simplest ac/dc converter that can be used with a piezoelectric generator. However, variations of the piezoelectric voltage amplitude at the ac side of a rectifier, while the dc-side voltage is retained fixed, can significantly reduce the amount of extracted power from a piezoelectric element [7], [8]. To enhance the amount of extracted power, various energy-harvesting circuits, based on active electronic components, have been suggested and demonstrated [7]–[14]. An evaluation of these circuits shows that, to have an efficient energy harvester circuit, reducing the nonscalable dissipations in the electronic components is of critical importance particularly for low-power applications such as wireless sensors.

Energy-harvesting circuits traditionally use full-bridge (FB) diode rectifiers combined with electronic control circuits. To enhance the extracted power, previous efforts have been mainly focused on electronic circuits that leverage one of these principles: adaptive control of the rectified dc voltage [7], [12], improving the extracted power using a nonadaptive circuit [8]–[11], or reducing the power loss in rectifying diodes [13], [14]. The demonstrated prototypes for energy-harvesting circuits based on FB rectifiers reveal that the nonadaptive circuits are more efficient than the adaptive one for low-power generators. However, they must be tuned for each device depending on the piezoelectric parameters and the device resistance. Therefore, the adaptive circuits are more desired since they can operate independent of the piezoelectric parameters and device loads. The limitations of existing adaptive circuits that use FB rectifiers are the following.

1) An FB rectifier needs a complex electronic interface, such as a microprocessor and an analog-to-digital (A/D) converter [7], [12], which dramatically reduces the efficiency of the energy harvester specially at low power (less than a few milliwatts).
2) It also needs an external sensing feedback, such as a current sensor [7], [12] or a displacement sensor (e.g., extra built-in electrodes on the piezoelectric beam) [8], [10], which increases the circuit's dissipations and complexity.

The work herein develops and demonstrates a viable adaptive piezoelectric energy-harvesting circuit based on a voltage-doubler (VD) rectifier which has been initially and briefly presented in [15]. The proposed circuit is suitable for low-power (0.5–5 mW) applications and overcomes the aforementioned limitations of the existing adaptive circuits. The circuit consists of a VD rectifier, a step-down converter, and a simple single-chip analog controller which allows stand-alone operation of the energy harvester circuit. As will be shown, the total power consumption of the controller unit is less than 0.05 mW, and the overall efficiency of the circuit prototype

Manuscript received January 29, 2009; revised November 17, 2009. First published December 4, 2009; current version published February 10, 2010.

A. Tabesh is with the Department of Electrical and Computer Engineering, Isfahan University of Technology, Isfahan 84156, Iran (e-mail: a.tabesh@utoronto.ca).

L. G. Fréchette is with the Microengineering Laboratory for MEMS, Department of Mechanical Engineering, Université de Sherbrooke, Sherbrooke, QC J1K 2R1, Canada (e-mail: lucf@alum.mit.edu).

Color versions of one or more of the figures in this paper are available online at http://ieeexplore.ieee.org.

Digital Object Identifier 10.1109/TIE.2009.2037648

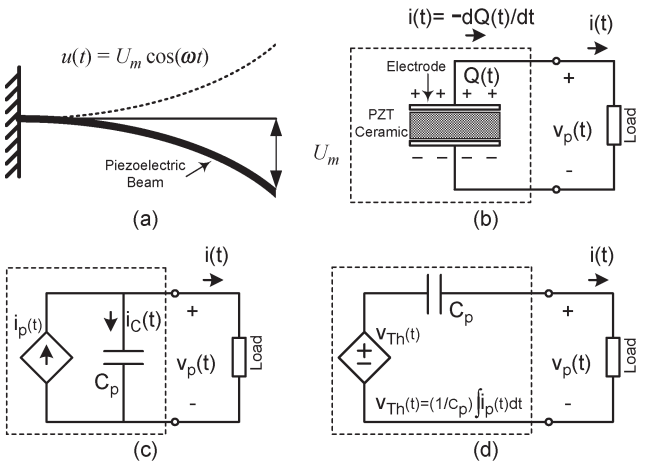

Fig. 1. (a) Schematic diagram of a vibrating piezoelectric beam (cantilever). (b) Electrical connection of the beam to a load. (c) Norton (current source) equivalent circuit of the piezoelectric energy harvester. (d) Thevenin (voltage source) equivalent circuit of the piezoelectric energy harvester.

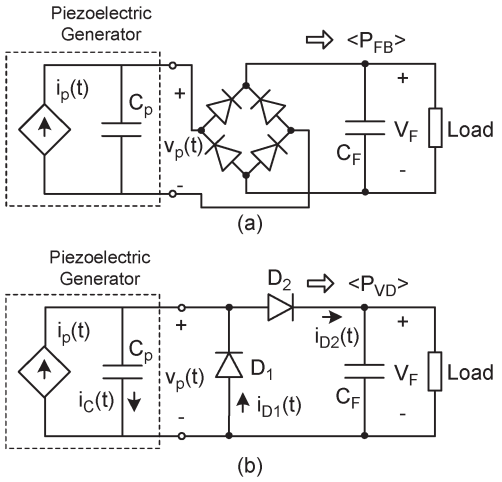

Fig. 2. (a) FB and (b) ac–dc VD rectifiers.

reaches 60%. The circuit improves the amount of extracted power from a piezoelectric generator independent of its operating frequency, vibration amplitude, and its geometry (capacitance). This feature of the circuit is of utmost importance for adaptive energy-harvesting devices that tune their resonant frequency to track the source vibrations. The limitations of the proposed energy-harvesting circuit are the following: 1) for a power range less than 0.5 mW, the circuit is not efficient mainly due to the control circuit's power loss, and 2) the VD rectifier of the circuit requires a filter capacitor with higher voltage level compared to an FB rectifier. This can limit the applications of the circuit for high voltages since the size and cost of a high-capacity storage are rapidly increased with voltage.

This paper is organized as follows. The next section first develops the vibrating piezoelectric model and establishes a condition for extracting maximum power from a piezoelectric generator connected to a VD rectifier. Then, the structure and functional operation of the proposed energy-harvesting circuitry will be discussed. Section III presents an experimental verification for the proposed circuitry via two test setups: a test setup for verification of the maximum power flow condition and another one for evaluation of the proposed energy-harvesting circuitry. Section IV identifies qualities for a viable energy-harvesting circuit that are as follows: efficiency, adaptivity, complexity, autonomy, and compatibility with microelectronics implementation. Using these criteria, the performance of the proposed circuitry will be evaluated and compared with other alternatives.

II. Energy-Harvesting Model and Circuitry

A. Piezoelectric Circuit Model

Fig. 1(a) and (b) shows the mechanical and electrical diagrams of a vibrating piezoelectric beam (cantilever) connected to a load. The electromechanical energy conversion mechanism of the beam can be modeled with a current source in parallel with a capacitor [6], [7], as shown in Fig. 1(c). Alternatively, the vibrating piezoelectric beam can be represented by a voltage source in series with a capacitance [the Thevenin equivalent circuit in Fig. 1(c)] with the equivalent parameters shown in Fig. 1(d). We use the improved small-deflection model presented in [6] to derive the components of this model. The static charge equation for a deflected piezoelectric beam is

$$Q = \Theta u + C_p v_p \tag{1}$$

where u is the deflection of the beam at the tip and v_p is the voltage across the piezoelectric electrodes. The coefficients Θ and C_p are the coupling and capacitance coefficients of the piezoelectric beam, respectively. They are functions of the piezoelectric properties and the beam geometry as elaborated in [6]. Using (1) and considering the sign convention in Fig. 1(b), the load current $(i = -dQ/dt)$ is given by

$$i(t) = -\frac{dQ}{dt} = -\Theta\frac{du}{dt} - C_p\frac{dv_p}{dt}. \tag{2}$$

A sinusoidal excitation $u = U_m\cos(\omega t)$, under a steady-state condition, generates a sinusoidal load current as

$$i(t) = \overbrace{\Theta\omega U_m \sin(\omega t)}^{i_p(t)} - \overbrace{C_p dv_p/dt}^{i_c(t)}. \tag{3}$$

Fig. 1(c) shows an equivalent circuit for the piezoelectric beam based on the load current in (3). In this circuit, the vibrating beam is represented with a capacitance C_p and a sinusoidal current source $i_p(t) = I_p\sin(\omega t)$, where the peak current $I_p = \Theta\omega U_m$ is proportional to the maximum tip deflection U_m and the vibrating frequency of the beam ω.

B. Rectifying Circuits and Optimal Power Flow

Fig. 2 shows two configurations for rectifying circuits: FB and VD diode rectifiers. For each configuration, the filter capacitor (C_F) is designed such that, for a specific load, the fluctuations of the filter voltage (V_F) are limited to a narrow band (typically less than 5% of the nominal dc voltage). For the FB configuration, the maximum rectified voltage occurs under no-load condition, and it is ideally equal to the peak open-circuit voltage at the piezoelectric terminals. This peak value based on the equivalent circuit in Fig. 1(c) is $V_{oc} = I_p/\omega C_p = \Theta U_m/C_p$, which is proportional to the maximum deflection U_m. When

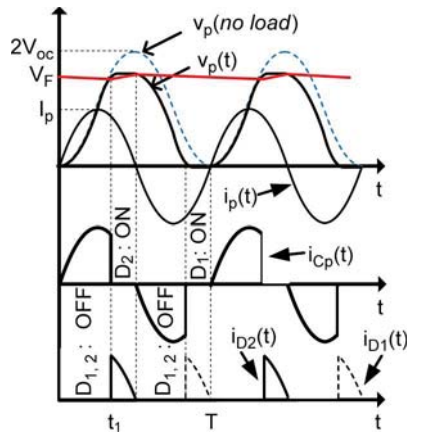

Fig. 3. Voltage and current waveforms of the VD rectifier.

the rectifier is connected to a load, the piezoelectric maximum voltage is limited to the filter voltage (i.e., $v_p(t) < V_F$). Ottman *et al.* [7] have analytically shown that, for an FB configuration, the maximum average power extracted from a piezoelectric device occurs when the rectifier voltage is one-half of the peak no-load voltage, and the maximum average power is

$$\langle P_{\rm FB}\rangle_{\max} = \frac{C_p\omega V_{\rm oc}^2}{2\pi} \quad \text{at} \quad V_F = \frac{V_{\rm oc}}{2} \tag{4}$$

where $P_{\rm FB}$ is the instantaneous extracted power and $\langle\cdot\rangle$ denotes its average value.

Herein, the theory of maximum power flow for the VD rectifier is developed. In the VD rectifier, the negative piezoelectric current passes through the diode D_1, and this diode does not allow v_p to become negative. Thus, only the positive piezoelectric current can charge up C_p starting from zero voltage ($v_p(0) = 0$). Under a no-load condition, the piezoelectric current totally charges up C_p, and the no-load peak voltage of the piezoelectric is

$$v_p\left(\frac{T}{2}\right) = \frac{1}{C_p}\int_0^{\frac{T}{2}} I_p\sin(\omega t)\,dt + \overbrace{v_p(0)}^{=0} = \frac{2I_p}{C_p\omega} = 2V_{\rm oc}. \tag{5}$$

Thus, the maximum filter voltage will also be $2V_{\rm oc}$. When a load is connected to the rectifier, the filter voltage becomes a rippled dc voltage (V_F in Fig. 3), and $V_F \le 2V_{\rm oc}$. Moreover, D_2 limits the piezoelectric voltage to be less than the filter voltage (i.e., $v_p(t) \le V_F \le 2V_{\rm oc}$). Since V_F is a positive voltage, the diodes D_1 and D_2 in Fig. 2(b) cannot conduct current simultaneously. Thus, the possible conditions for the diodes are the following:

1) (D_1: off, D_2: off) when the piezoelectric beam charges or discharges its inherent capacitor C_p;
2) (D_1: off, D_2: on) when the positive current of the piezoelectric delivers power to the filter and the load;
3) (D_1: on, D_2: off) when the negative current of the piezoelectric flows through D_1.

The first graph in Fig. 3 shows the waveforms of the piezoelectric voltage $v_p(t)$, the current $i_p(t)$, and the filter (rectified) voltage V_F. The graph also depicts the piezoelectric no-load voltage ($v_p(no\ load)$) as a reference signal. The second and third graphs in Fig. 3 show the currents of the piezoelectric capacitor (i_{C_p}) and diodes (i_{D_1} and i_{D_2}) corresponding to the filter voltage V_F. When D_2 is off, the filter capacitor supplies the total load current; thus, V_F drops. When D_2 conducts, the piezoelectric current charges the filter capacitor, which increases V_F. Ideally, diodes with zero voltage drops are suddenly turned on/off, as shown in Fig. 3, and the nonzero portions of i_{C_p}, i_{D_1}, and i_{D_2} are the same as the piezoelectric current i_p. In practice, however, $v_p(t)$ will have smooth transitions (corners) determined by the nonlinear $v-i$ characteristic of the diodes, and as it will be discussed later, there is a small shift in the voltage waveforms due to the voltage drops across nonideal diodes (see Fig. 6). The instantaneous extracted power from the VD rectifier is $P_{\rm VD}(t) = V_F i_{D_2}(t)$. Considering a period T, i_{D_2} is equal to $I_p\sin(\omega t)$ for $t_1 < t < T/2$, and it is zero ($i_{D_2} = 0$) for the rest of the period. Thus, the average extracted power from the piezoelectric is

$$\langle P_{\rm VD}\rangle = \frac{1}{T}\int_0^T V_F i_{D_2}(t)\,dt = \frac{V_F}{T}\int_{t_1}^{\frac{T}{2}} I_p\sin(\omega t)\,dt. \tag{6}$$

We can find the integral by changing the variable of integration $dt = (1/\omega)\,d\omega t$ and by substituting $T = 2\pi/\omega$ in (6) as

$$\langle P_{\rm VD}\rangle = \frac{V_F}{2\pi}\int_{\omega t_1}^{\pi} I_p\sin(\omega t)\,d\omega t = \frac{V_F I_p}{2\pi}\left(1+\cos(\omega t_1)\right). \tag{7}$$

To determine the average power, we need to find $\cos(\omega t_1)$, which can be obtained from the voltage–current equation of the piezoelectric capacitor as given by

$$v_p(t_1) = V_F = \frac{1}{C_p}\int_0^{t_1} i_{C_p}(t)dt + v_p(0). \tag{8}$$

Since $i_C = i_p$ for $0 < t < t_1$ and $v_p(0) = 0$, we deduce

$$V_F = \frac{1}{C_p\omega}\int_0^{\omega t_1} I_p\sin(\omega t)d\omega t = \frac{1-I_p\cos(\omega t_1)}{C_p\omega}. \tag{9}$$

Solving (9) for $\cos(\omega_1 t)$ and substituting the solution in (7) yield

$$\langle P_{\rm VD}\rangle = \frac{V_F}{2\pi}(2I_p - C_p\omega V_F). \tag{10}$$

The extracted average power is maximum when

$$\frac{d}{dV_F}\langle P_{\rm VD}\rangle = 0 \Rightarrow V_F = \frac{I_p}{C_p\omega} = V_{\rm oc}. \tag{11}$$

Thus, the maximum extracted average power is

$$\langle P_{\rm VD}\rangle_{\max} = \frac{C_p\omega V_{\rm oc}^2}{2\pi} \quad \text{at} \quad V_F = V_{\rm oc}. \tag{12}$$

Comparing (4) and (12) reveals that, ideally, the maximum extracted powers by the FB and VD rectifiers are the same. However, the VD rectifier delivers the power at the higher

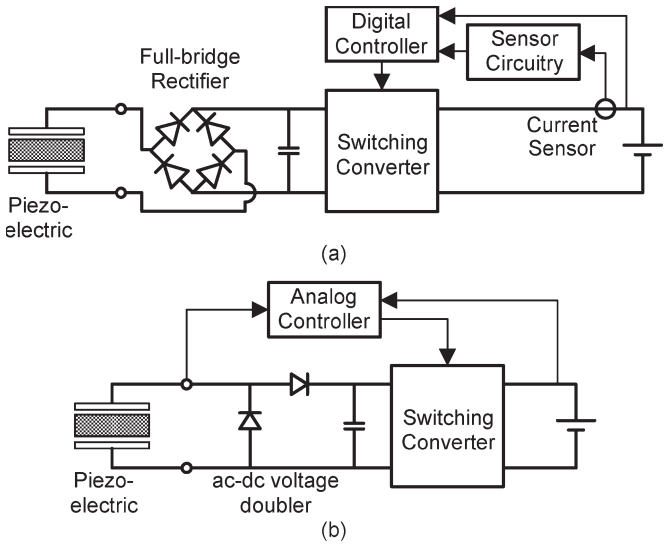

Fig. 4. Schematic diagrams for adaptive energy harvester circuits. (a) FB-based circuit using output current as a feedback. (b) Proposed circuit using piezoelectric voltage as a feedback.

voltage ($V_{F_{\rm VD}} = V_{\rm oc}$), which is twice that of the FB ($V_{F_{\rm FB}} = V_{\rm oc}/2$), which means that the VD rectifier can extract the maximum power at a lower current. In practice, extracting power at a lower current means less power dissipations in diodes due to the built-in voltages of the diodes. Furthermore, the VD rectifier uses two diodes less than the FB that, in turn, will further reduce the total diode power dissipations. Thus, the VD rectifier is inherently more efficient than the FB rectifier. This merit will be experimentally verified in Section III.

C. Switching Circuit and Power Flow Controller

The piezoelectric voltage can vary in a wide range due to the variation of mechanical vibration excitations, while on the other hand, electronic devices require a constant regulated voltage. To retain maximum power extraction, one approach is to adaptively adjust the rectified voltage with respect to the piezoelectric open-circuit voltage ($V_{\rm oc}$) by using a dc–dc power converter. The block diagram of this method for the FB rectifier is shown in Fig. 4(a). Since $V_{\rm oc}$ is not a measurable signal when the piezoelectric is connected to a load, the output current is typically measured and used as a feedback signal to the controller. The digital controller maximizes the extracted power by adjusting the duty cycle of the switching converter based on the monitored output current variations [7], [12].

We present an alternative energy-harvesting circuit for the VD rectifier, as shown in Fig. 4(b). This circuit directly uses the piezoelectric voltage as a control signal, which is critical for the development of a low-power control circuit: Other harvesting circuits use external sensors to create sensing feedbacks that need additional processing circuits.

The controller in Fig. 4(b) adjusts the rectified voltage V_F by turning on/off the switching converter. The goal of using a controller is to maintain $V_F = V_{\rm oc}$ regardless of the variations of $V_{\rm oc}$, to maximize the extracted power based on (12). Since the energy harvester is connected to a load, $V_{\rm oc}$ is not directly measurable. Thus, the controller satisfies the condition $V_F = V_{\rm oc}$ by measuring and adjusting the duty cycle of $v_p(t)$ (and $V_{\rm cm}$ in Fig. 5). Fig. 5 shows the details of the proposed circuitry through a simplified circuit diagram of the switching converter, the rectifier circuit, and the analog controller. The switching circuit is a step-down (buck) converter since the piezoelectric open-circuit voltage ($V_{\rm oc}$) is often higher than the voltage of the battery. The waveforms of the piezoelectric voltage $v_p(t)$ corresponding to an arbitrary filter voltage V_F are shown in Fig. 6. The maximum of $v_p(t)$ can change between two extremes from V_b to $2V_{\rm oc}$, and the waveforms of $v_p(t)$ corresponding to these extremes are also shown in Fig. 6. When the diode D_2 is on, the piezoelectric voltage is $v_p = V_F + V_{D_2}$, where V_{D_2} is the voltage drop across D_2. For $v_p(t) < 0$, the diode D_1 is on, and thus, $v_p = -V_{D_1}$, where V_{D_1} is the voltage drop across D_1. This negative voltage enables comparator C_1 to generate the $V_{\rm cm}$ pulse with a duty cycle proportional to the time frame in which D_1 is off, as shown in Fig. 6. The controller, which is simply an RC low-pass filter, generates the average of $V_{\rm cm}$ denoted by $V_{\rm ct}$ (the rippled dc voltage) in Fig. 6. $V_{\rm ct}$ varies correspondingly to the duty cycle of $V_{\rm cm}$. Then, C_2 compares $V_{\rm ct}$ with a reference signal ($V_{\rm ref1}$) to generate a gating signal which turns on/off the oscillator (C_3). The waveforms depict a situation in which $V_F \geq V_{\rm oc}$; therefore, $V_{\rm ct} < V_{\rm ref1}$ in Fig. 6. The gating signal, in the closed-loop feedback system in Fig. 5, changes the duty cycle of $V_{\rm cm}$ to regulate $V_{\rm ct}$ at $V_{\rm ref1}$. The frequency of the oscillator determines the switching circuit operating frequency. The frequency is selected well above the cutoff frequency of the controller to avoid overlaps among switching circuit transients and the transients due to the controller's on/off commands. The algorithm of the controller is summarized in the simple flowchart in Fig. 6.

Theoretically, $V_F = V_{\rm oc}$ is corresponding to the $V_{\rm cm}$ pulse with a duty cycle of 50% since $V_{F_{\max}} = 2V_{\rm oc}$ under a no-load condition. Practically, when $V_F = V_{\rm oc}$, the duty cycle of $V_{\rm cm}$ is not exactly 50% (but close to it) due to the voltage drops across the diodes. The control circuit can be tuned to maintain $V_F = V_{\rm oc}$ by tuning $V_{\rm ref1}$ since $V_{\rm ref1}$ determines a reference for the duty cycle of $V_{\rm cm}$. The comparator chip is supplied by the fixed battery voltage V_b that means that the duty cycle of $V_{\rm cm}$ can be controlled independent of $V_{\rm oc}$. Therefore, the controller is able to maintain $V_F = V_{\rm oc}$ independent of the amplitude and frequency of the piezoelectric voltage $v_p(t)$. This capability will be experimentally verified using a test setup in the following section.

III. Experimental Verification

The proposed rectifying circuit and switching converter were experimentally investigated using two test setups. In the first test, we investigated the effect of rectified voltage on the extracted power from a piezoelectric generator without using the adaptive switching circuit. The second test setup demonstrates the prototype of the proposed energy-harvesting circuit and investigates the operation of its controller and switching circuits for extracting maximum power from the piezoelectric generator.

A. Test 1: Piezoelectric Generator With Simple Rectifiers

Fig. 7 shows the schematic diagram of the first setup for testing the FB and VD rectifiers to compare the power losses

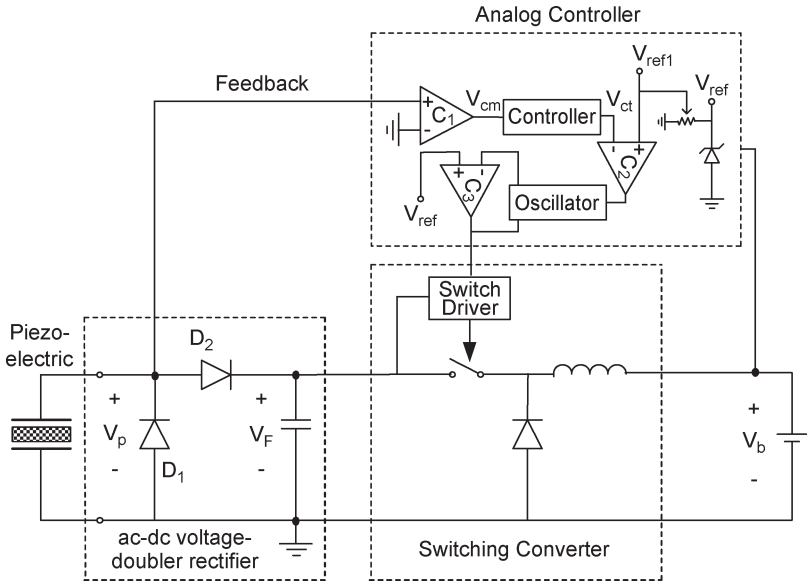

Fig. 5. Functional diagram of the proposed circuit.

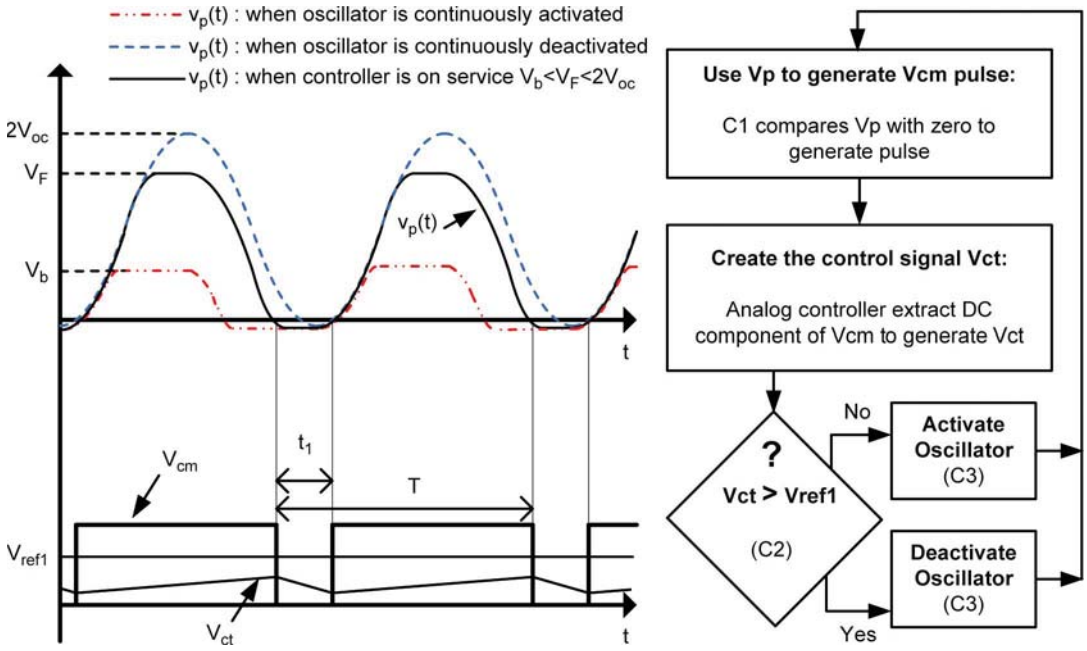

Fig. 6. (Left) Signal waveforms of the analog controller circuit and (right) the flowchart of the controller's algorithm.

of the diodes in these configurations. The prototype for this setup was implemented and tested using a piezoelectric actuator as a mechanical vibration source that drives a piezoelectric generator. A two-layer piezoelectric bending beam (cantilever configuration) was used as the piezoelectric generator (Quick-Mount Q220-A4-303YB of Piezo Systems, Inc.). A similar beam was also used as the piezoelectric shaker in actuator mode. The beam was made of a PZT-5A4E material, polled for series operating mode. The beam dimensions were the following: 31.8-mm length, 12.7-mm width, and 0.51-mm thickness (the center brass shim thickness is 0.13 mm). The actuator and generator beams were fixed at one end and simply contacted face to face at the free end, without using any adhesive material. The frequency and the amplitude of the actuator were controlled with a function generator connected to the beam via a power amplifier. The actuator was sinusoidally excited by a function generator (Agilent Technologies, model: 33220A) connected to a power amplifier (piezo linear amplifier EPA-105-115 of Piezo Systems, Inc.). The vibrating frequency of the actuator was fixed at 250 Hz (resonant frequency of the beam), and the exciting voltage amplitude was adjusted to obtain the desired peak open-circuit voltages during these tests. We monitored the tip deflection of the beam using an optical laser displacement probe (Philtec, Inc., model: D6). Small-signal diodes (2N4148) were used to implement the rectifying circuit of both FB and VD configurations. The rectified dc side was directly connected to a variable dc power supply that behaves as a battery and can be a sink or a source for low electric current at a fixed voltage level. The average currents of the rectifiers were measured using a current sensor made

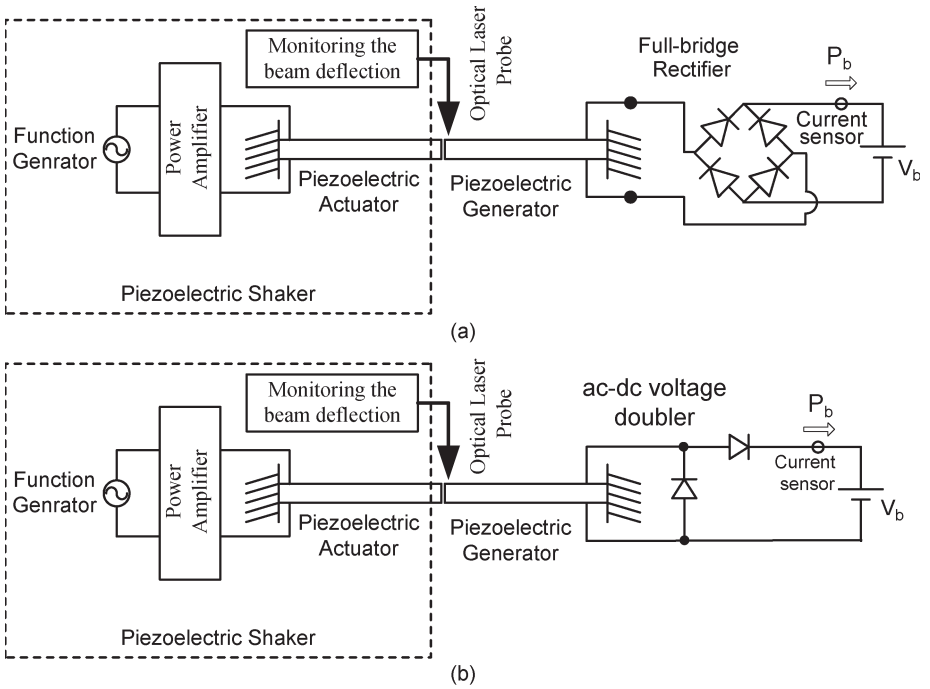

Fig. 7. Schematic diagrams of the first setup for the (a) FB and (b) VD rectifiers.

of a 100-Ω resistor in parallel with a 1-μF ceramic capacitor. The average current was proportional to the average voltage across the sensor's resistor which was measured by a digital multimeter (Extech Instruments Corporation, model: 570). The measured average value of the current sensors (Fig. 7) was used to calculate the extracted power from the vibrating piezoelectric beam at various rectified dc supply voltages ranging from 0 up to maximum 30 V. Each test was repeated for three peak open-circuit voltages: $V_{\rm oc} = 5$, 10, and 15 V. Fig. 8 shows the graphs of the extracted power P_b versus the rectified voltage V_b for the FB and VD rectifiers. The first graph confirms that, for the FB rectifier, the maximum power is extracted at a dc supply voltage close to half of the peak open-circuit voltage. The second graph shows that, for the VD rectifier, the maximum extracted power occurs around the peak open-circuit voltage. Based on (4) and (12), ideally, one expects the same peak average power in the first and second graphs in Fig. 8. However, the graphs show that the extracted power by the VD rectifier is higher than that by the FB rectifier. The reason is that the VD rectifier extracts maximum power at a higher voltage (lower current) and that it uses two diodes less than the FB rectifier.

The third graph in Fig. 8 compares the power losses of the FB and VD rectifiers $P_{\rm diodes}$, which are normalized with respect to the extracted power P_b. The diode power losses $P_{\rm diodes}$ are calculated based on their measured average voltages and currents. The graphs show that the losses for the FB rectifier are higher than those for the VD rectifier specially at the low extracted power. The power losses of the diodes can be further decreased by using diodes with lower p-n junction voltage drops (Schottky diodes); thus, for the next circuit (Fig. 9), we used Schottky diodes. The test results of the first setup (Fig. 7) with typical small-signal diodes show that, for the power range of 0.5–5 mW, the maximum power losses due to diodes in a worst case are less than 5% of the total extracted power for the VD rectifier. As it will be discussed in the next test, the switching circuit's power losses are about 40% of the total power. Thus, the diodes do not significantly impact on the efficiency of the energy-harvesting circuit.

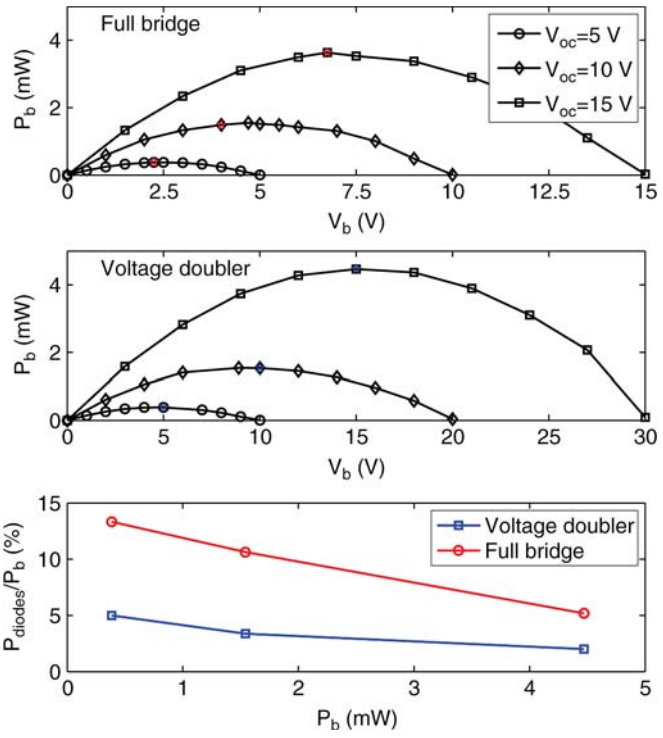

Fig. 8. Test results obtained from the first setup.

B. Test 2: Adaptive Energy-Harvesting Circuitry

This experiment examined the role of the switching circuit to improve the extracted power from the piezoelectric element. For this test, first, we directly connected the fixed 2.57-V

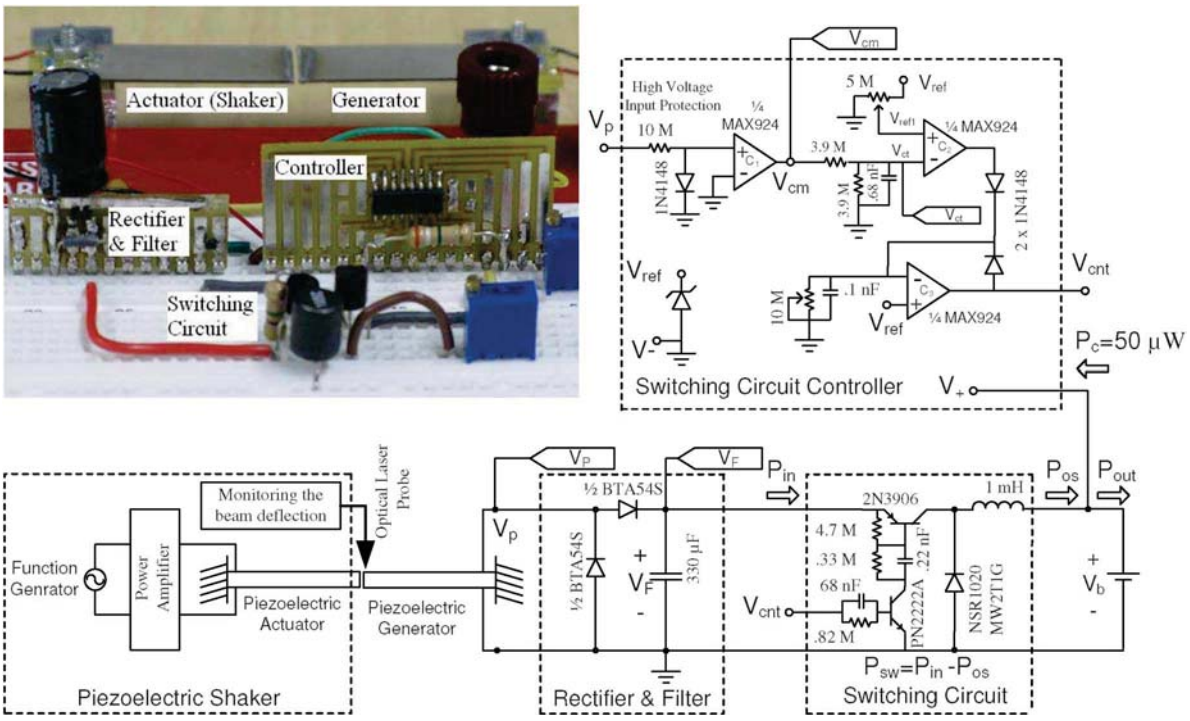

Fig. 9. Schematic diagram of the proposed low-power energy-harvesting circuit and a picture of the prototype.

rechargeable batteries (two series AA-size Sony 2700mAh Ni-MH) to the rectifier and measured the extracted power at different piezoelectric open-circuit voltages ranging from $V_{\rm oc} =$ 3 to 20 V. Then, we used the switching circuit, as shown in Fig. 9, and repeated the test. For each test, the piezoelectric was disconnected from the load at the beginning of the test to adjust and measure $V_{\rm oc}$. The electronic circuit for the energy harvester was composed of Schottky diodes (for the ac–dc rectifier and switching circuits), bipolar junction transistors (BJTs) as the switch and driver, and a 1-mH inductor for the step-down converter (Fig. 9). BJTs are selected instead of MOSFETs since a MOSFET requires high-side drivers (an inverting gate in the simplest case). At present, off-the-shelf low-power MOSFETs and drivers need more power than the BJT configuration, which is shown in Fig. 9. We used the analog comparator chip *MAX*924 by *Maxim* to build the control unit. This chip includes four ultralow-power comparators (10 μA, 2.5 V) and a built-in reference voltage. The chip's supply voltage ranges from 2.5 to 15 V, and in this circuit, the supply voltage of the chip is $V_b = 2.57$ V. However, since the piezoelectric voltage (v_p) can be higher than 15 V, we used a protection circuit for this input, as shown in Fig. 9.

The details of the control circuit and the sawtooth generator components of the controller are shown in Fig. 9. The average input power to the switching circuit $P_{\rm in}$, the switching circuit total output power $P_{\rm os}$, and the controller power consumption P_C were calculated based on the measured average currents at the corresponding points. Fig. 10 shows the comparison of the captured waveforms from the experimental setup (V_p, $V_{\rm cm}$, $V_{\rm ct}$, and V_F in Fig. 9) with the signals that were used for analytical analysis (denoted by dashed lines in Fig. 10). The captured signals have close matches with the assumed waveforms in Fig. 6 (reshown by dashed lines in Fig. 10) which verify the validity of the assumed signals for analysis.

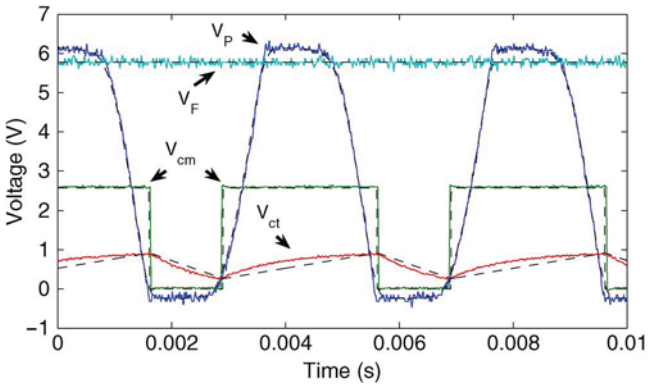

Fig. 10. (Solid lines) Captured waveforms from the experimental setup versus (dashed lines) estimated signals for analysis.

The superimposed noises on the signals are mainly due to the transients of switching circuits. The controller is a low-pass filter (RC integrator) which mitigates the adverse effects of noises by limiting the bandwidth of the closed-loop control circuit.

The results of the calculated powers and efficiency of the circuit are summarized in Figs. 11 and 12, showing that the proposed energy-harvesting circuit successfully and efficiently charges the battery. The graphs in Fig. 11 compare the power of a directly connected battery with the output power of the switching circuit. As Fig. 11 shows, for an extracted power less than 0.5 mW (corresponding to $V_{\rm oc} < 8$ V for this prototype), the extracted power using a direct connection is higher than the one using the power circuit due to switching circuit power losses. However, for an extracted power higher than 0.5 mW $(V_{\rm oc} \geq 8$ V), the useful output power of the switching circuit rapidly increases up to twice that of the directly connected batteries since the switching circuit adaptively matches the

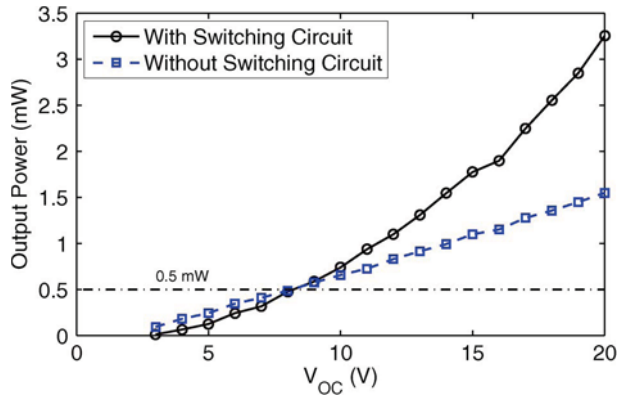

Fig. 11. Test results that compare the useful output power ($P_{\rm out}$) of the piezoelectric generator with and without the switching circuit.

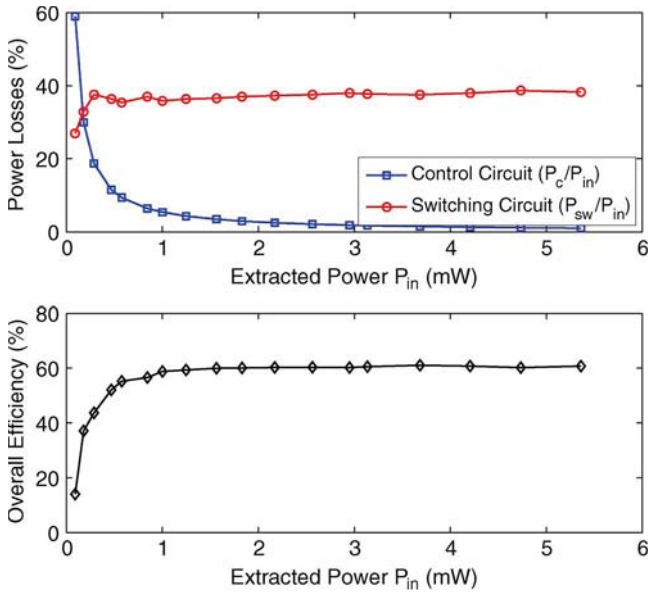

Fig. 12. Power losses and efficiency of the proposed circuit.

rectified voltage with the open-circuit voltage. The first graph in Fig. 12 compares the normalized power losses of the switching circuit and the control circuit ($P_{\rm sw}/P_{\rm in}$ and $P_c/P_{\rm in}$ in Fig. 9) versus the extracted power ($P_{\rm in}$). The power losses are normalized with respect to $P_{\rm in}$ to be readily comparable. The graph shows that, for an extracted power above 0.5 mW, power losses are dominantly determined by the switching circuit, and the contribution of the control circuit in power dissipation becomes negligible. The last graph in Fig. 12 depicts the overall efficiency of the power circuit ($P_{\rm out}/P_{\rm in}$ in Fig. 9) that asymptotes to 60% at a power level of 5 mW. This efficiency is satisfactory for this prototype test circuit since the reported efficiencies of step-down switching power converters rapidly drop below 50% at a power level less than 10 mW [16].

To evaluate the adaptivity (robustness) of the controller versus the variations of the input voltage amplitude and its frequency, two individual tests were preformed using the setup. A function generator in series with a 47-nF capacitor was used instead of the piezoelectric beam to enable measurement of $V_{\rm oc}$ for adaptivity test since $V_{\rm Th}$ in the piezoelectric equivalent circuit [Fig. 1(d)] is not accessible for measurement. In the first test, the frequency was fixed at 250 Hz, and the controller was

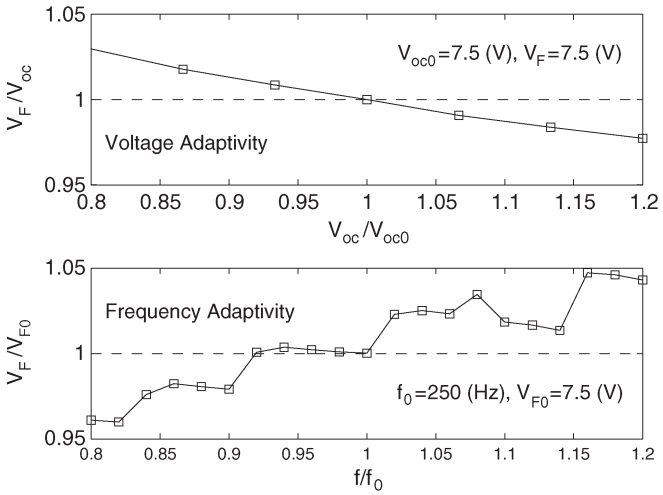

Fig. 13. Adaptivity of the controller versus voltage and frequency.

precisely tuned such that $V_{\rm oc} = V_F$ at the center point $V_{{\rm oc}_0} = V_{F_0} = 7.5$ V. Then, the voltage ratio $V_{\rm oc}/V_{{\rm oc}_0}$ was changed by $\pm 20\%$, and V_F was measured with respect to $V_{\rm oc}$. The first graph in Fig. 13 shows the deviations of $V_F/V_{\rm oc}$ from the ideal behavior (depicted by a dashed line) which are less than 5% for a $\pm 20\%$ change in the input voltage. In the second test, $V_{\rm oc}$ was retained constant at 7.5 V, and the controller was precisely tuned at the center point $f_0 = 250$ Hz and $V_{F_0} = 7.5$ V. Then, the frequency ratio f/f_0 was changed by $\pm 20\%$, and we measured the variation of V_F due to the change of frequency. The second graph in Fig. 13 compares V_F/V_{F_0} with its ideal value (dashed line), showing that the deviations due to change of frequency are less than 5% in V_F/V_{F_0}. The conclusion is that the controller is adequately stable and robust (adaptive in this context) to maintain $V_F \simeq V_{\rm oc}$ independent of the variations of the amplitude and frequency.

IV. Performance Evaluation

A performance evaluation of an energy-harvesting circuitry has been conventionally performed by comparing the circuit with the standard FB rectifier [Fig. 7(a)] [7]–[14]. Using this approach, improvement rates of 400% [7], 325% [9], 900% [10], and 37% [14] have been reported for various energy-harvesting circuitries. However, these improvement rates are not comparable for two reasons: First, the measurement tests were performed at different power levels, and second, the total power dissipation of the electronic circuits has not been considered in some configurations. To evaluate the energy-harvesting circuits more accurately, we first define the following five criteria of an ideal energy-harvesting circuitry as follows.

1) **Efficiency**: The circuitry must be adequately efficient such that power losses are small compared to the input power. To realistically evaluate an energy-harvesting circuit, nonscalable power consumption of all electronic circuitries, including a sensing unit, a switching power supply, and a controller unit, must be separately calculated and taken into account. The circuit efficiency is best expressed versus a range of the extracted power from the piezoelectric generator rather than a single operating point.

TABLE I
COMPARING THE FEATURES OF DIFFERENT PIEZOELECTRIC ENERGY HARVESTERS

Method	Features and Performance Evaluation
1- Simple passive rectifier (Standard full-bridge rectifier, Fig. 7(a))	Low efficiency; Non-adaptive; Stand-alone operation; Sensorless; No external supply required; Highly compatible for micro-scale integration
2- Synchronized rectifier (Full-bridge or voltage-doubler) [14]	Improve efficiency (37% higher) against Method 1 but the efficiency is still low since the circuit is not adaptive; Stand-alone operation; Single supply voltage, Sensorless; Implemented and demonstrated as a CMOS micro-chip;
3- Optimized energy harvester for a full-bridge rectifier using step-down converter [9]	Non-adaptive; Stand-alone (for $P_{in} > 10\ mW$ and $V_{oc} > 30\ V$); No external sensor; Multi supply voltage; Efficiency: ($< 20\%$ for $P_{in} < 5\ mW$, 60% for $P_{in} > 10\ mW$); Fairly compatible for micro-scale integration;
4- Adaptive energy harvester for a full-bridge rectifier using step-down converter [7], [12]	External Sensor (current); Adaptive; Not stand-alone; Need multi supply voltage (for sensing circuit); Efficiency and the total circuits power losses have not been reported; Fairly compatible for micro-scale integration;
5- Synchronized switch harvesting [8], [10]	External Sensor (to determine switching time with respect to displacement); Non-adaptive; Stand-alone; Possibly needs multi supply voltage (for sensing circuit, details of circuitry has not been provided); Efficiency: 70% (Peak power: 300 mW; Circuit consumes 5% of extracted power (Max. power loss: 15 mW)); Fairly compatible for micro-scale integration;
6- Buck-boost sensorless energy harvester [11]	Sensorless; Non-adaptive; Stand-alone; Single supply voltage; Efficiency: above 84% for the power range 0.2-1.5 mW (for a given load and piezoelectric parameters); Fairly compatible for micro-scale integration.
7- Adaptive energy harvester using voltage-doubler rectifier as described in this paper	Stand-alone (for $P_{in} > 0.5$ mW and $V_{oc} > 8\ V$); Adaptive; No external sensor; Single supply voltage; Efficiency: 60% for $P_{in} > 0.5$ mW (independent of load and piezoelectric parameters); Fairly compatible for micro-scale integration.

2) **Stand-alone operation**: This characteristic means that an energy-harvesting circuitry can operate independent of the other components of an end-user device (e.g., the power management unit of a wireless sensor node). An integration of an energy-harvesting circuit with the other electronic components of an end-user device is not necessarily an efficient power management approach. For example, for a wireless sensor node in sleep mode, using a stand-alone energy harvester circuit allows switching off a major part of the node's microprocessor unit, in addition to the high-power radio unit, to save more energy.
3) **Circuit complexity**: It is of great importance that an energy-harvesting circuit be able to operate with a single supply voltage typically at 3 V. Using complex circuits including sensing units (e.g., op-amps), switching circuit drivers (e.g., MOSFET high-side drivers) and A/D converters (when using digital controllers) often need multiple supply voltages [7], [9]. In high-power applications (> 1 W), it is readily possible to convert a single supply voltage into any positive or negative voltage level using high-efficiency converters that are even available as discrete electronic components. However, in low-power applications, multiple supply voltage levels significantly reduce the efficiency of an energy-harvesting circuit due to the nonscalable power losses.
4) **Adaptivity**: The circuitry should be able to adjust the rectified voltage to ensure maximum power extraction. Without the adaptivity feature, an energy-harvesting circuit is inefficient since the vibration amplitude of a beam is not fixed, and therefore, the flow of power is not optimum.
5) **Microscale compatibility**: This criterion illustrates the potential for integration of an energy-harvesting circuit, which improves the overall efficiency and energy density and reduces the cost. The simplicity of the circuit and avoiding external sensors for adaptive control are important factors that determine the microscale compatibility of an energy-harvesting circuit.

Using these criteria, the proposed circuitry in this paper is compared, along with six other energy-harvesting circuits, in Table I. Comparing the listed features, we conclude the following.

1) The FB configuration is the only efficient option when the extracted power is very low (< 0.1 mW). The reason is that power consumption of any electronic interface for adaptive circuits (based on available technology at the present time) will be higher than the total generated power.
2) The nonadaptive energy-harvesting circuits are suitable alternatives when they are specifically designed for a given piezoelectric geometry connected to a fixed resistive load. These circuits can be more efficient than adaptive circuits, specially for the range of 0.1–1 mW.
3) For an end-user device with a fixed voltage (more common scenario), the adaptive circuits can be considered as suitable energy-harvesting configurations. The reason is that, at a fixed voltage, the load current dictates the equivalent resistance of the load which is variable and may

not be within its optimal range. Then, the best adaptive method can be selected based on other criteria such as the following: efficiency (which depends on the level of output power) and simplicity of the circuit implementation.

Considering the aforementioned classification and comparing the features of the circuits (Table I) show that the proposed circuitry is a promising energy harvester for low-power applications with variable load/excitation currents.

V. Conclusion

An efficient circuit was presented and demonstrated for harvesting energy from a vibrating piezoelectric element at low power levels, above 0.5 mW. Compared to a simple FB rectifier, the proposed circuit enhances the extracted power from a vibrating piezoelectric element with an increasing rate proportional to the extracted power. This improvement rate is at least a factor of two at an output power above 3 mW. The nonscalable power loss of the electronic circuitry is less than 0.05 mW, and the overall efficiency is about 60% for power levels above 0.5 mW.

This paper elaborates criteria for comparing the performance of energy-harvesting circuits. These criteria evaluate an energy-harvesting circuit considering broad aspects of efficiency, adaptivity, circuit complexity, autonomy, and compatibility for microscale implementation. The significant features of the proposed circuit in comparison with other available configurations are the following: 1) It controls the rectified voltage adaptively and without using an external sensing circuit to maximize the extracted power from the piezoelectric element; 2) its controller consists of only one chip with a single supply voltage that simplifies the implementation of the circuit as a stand-alone circuit; and 3) the controller's circuit is efficient due to its low power consumption. The proposed circuit herein can be further improved by designing more efficient switching converters. This would require the design of dedicated switches and drivers that are optimized for ultralow-power applications.

The proposed circuit is useful for efficient energy conversion of vibrating piezoelectric generators with application to low-power portable/wireless devices. An efficient piezoelectric energy harvester either increases the lifetime of the battery of a device or alternatively can be used as a long-life power supply for self-powered remote sensor nodes.

References

[1] S. Roundy and P. K. Wright, "A piezoelectric vibration based generator for wireless electronics," *Smart Mater. Struct.*, vol. 13, no. 5, pp. 1131–1142, Oct. 2004.

[2] G. Poulin, E. Sarraute, and F. Costa, "Generation of electric energy for portable devices: Comparative study of an electromagnetic and a piezoelectric system," *Sens. Actuators A, Phys.*, vol. 116, no. 3, pp. 461–471, Oct. 2004.

[3] S. W. Arms, C. P. Townsend, D. L. Churchil, J. H. Galbreath, and S. W. Mundell, "Power management for energy harvesting wireless sensors," in *Proc. SPIE Int. Symp. Smart Struct. Smart Mater.*, San Diego, CA, Mar. 2005, vol. 5763, pp. 267–275.

[4] N. Elvin, A. Elvin, and D. H. Choi, "A self-powered damage detection sensor," *J. Strain Anal. Eng. Des.*, vol. 38, no. 2, pp. 115–124, Mar. 2003.

[5] S. R. Anton and H. A. Sodano, "A review of power harvesting using piezoelectric materials (2003–2006)," *Smart Mater. Struct.*, vol. 16, no. 3, pp. R1–R21, Jun. 2007.

[6] A. Tabesh and L. G. Fréchette, "An improved small-deflection electromechanical model for piezoelectric bending beam actuators and energy harvesters," *J. Micromech. Microeng.*, vol. 18, no. 10, pp. 104 009-1–104 009-12, Oct. 2008.

[7] G. K. Ottman, H. F. Hofmann, A. C. Bhatt, and G. A. Lesieutre, "Adaptive piezoelectric energy harvesting circuit for wireless remote power supply," *IEEE Trans. Power Electron.*, vol. 17, no. 5, pp. 669–676, Sep. 2002.

[8] E. Lefeuvre, A. Badel, C. Richard, L. Petit, and D. Guyomar, "A comparison between several vibration-powered piezoelectric generators for standalone systems," *Sens. Actuators A, Phys.*, vol. 126, no. 2, pp. 405–416, Feb. 2006.

[9] G. K. Ottman, H. F. Hofmann, and G. A. Lesieutre, "Optimized piezoelectric energy harvesting circuit using step-down converter in discontinuous conduction mode," *IEEE Trans. Power Electron.*, vol. 18, no. 2, pp. 696–703, Mar. 2003.

[10] D. Guyomar, A. Badel, E. Lefeuvre, and C. Richard, "Toward energy harvesting using active materials and conversion improvement by nonlinear processing," *IEEE Trans. Ultrason., Ferroelectr., Freq. Control*, vol. 52, no. 4, pp. 584–595, Apr. 2005.

[11] E. Lefeuvre, D. Audigier, C. Richard, and D. Guyomar, "Buck–boost converter for sensorless power optimization of piezoelectric energy harvester," *IEEE Trans. Power Electron.*, vol. 22, no. 5, pp. 2018–2025, Sep. 2007.

[12] Y. Ammar, A. Buhrig, M. Marzencki, B. Charlot, S. Basrour, K. Matou, and M. Renaudin, "Wireless sensor network node with asynchronous architecture and vibration harvesting micro power generator," in *Proc. Joint Conf. Smart Objects Ambient Intell.*, Grenoble, France, Oct. 2005, pp. 287–292.

[13] J. Han, A. V. Jouanne, T. Le, K. Mayaram, and T. S. Fiez, "Novel power conditioning circuits for piezoelectric micro power generators," in *Proc. IEEE APEC*, 2004, vol. 3, pp. 1541–1546.

[14] T. T. Le, J. Han, A. Jouanne, K. Mayaram, and T. S. Fiez, "Piezoelectric micro-power generation interface circuits," *IEEE J. Solid-State Circuits*, vol. 41, no. 6, pp. 1411–1420, Jun. 2006.

[15] A. Tabesh and L. G. Fréchette, "Ultra low power stand-alone circuitry for harvesting energy from a micro-power piezoelectric generator," in *Proc. PowerMEMS/microEMS*, Sendai, Japan, Nov. 2008, vol. 1, pp. 289–292.

[16] S. Musunuri and P. L. Chapman, "Improvement of light-load efficiency using width-switching scheme for CMOS transistors," *IEEE Power Electron. Lett.*, vol. 3, no. 3, pp. 105–110, Sep. 2005.

Ahmadreza Tabesh (M'05) received the Ph.D. degree in energy systems from the University of Toronto, Toronto, ON, Canada, in 2005.

From 2006 to 2009, he was a Postdoctoral Fellow in the Microengineering Laboratory for MEMS, Department of Mechanical Engineering, Université de Sherbrooke, Sherbrooke, QC, Canada. He is currently an Assistant Professor at Isfahan University of Technology, Isfahan, Iran. His area of research includes renewable energy systems and microelectromechanical systems (MEMS) for energy harvesting (power MEMS).

Luc G. Fréchette (M'04) received the Ph.D. degree in aeronautics and astronautics from the Massachusetts Institute of Technology, Cambridge, in 2000 for the design and fabrication of MEMS-based energy conversion microsystems.

He was with Columbia University, New York, NY, for four years. He is currently the Canada Research Chair in Microfluidics and Power MEMS and a Professor at the Université de Sherbrooke, Sherbrooke, QC, Canada. His area of expertise is MEMS with emphasis on thermal and fluidic applications for sensing, actuating, and integrated microsystems. His research activities include microfuel cells, MEMS heat engines (microturbines), microenergy harvesting, and microfluidics, as well as MEMS sensors and actuators for cooling and harsh environments. He has written over 60 technical and scientific publications.

Dr. Fréchette has been actively involved in the organization of international conferences (PowerMEMS, ASME International Mechanical Engineering Congress and Exposition, and Transducers).